Deng *et al. Energy Mater.* **2025**, *5*, 500103
DOI: 10.20517/energymater.2024.299

Energy Materials

Article

Open Access

Check for updates

Design of a polymer electrolyte membrane for enhanced zinc anode stability in reversible aqueous zinc-ion batteries

Qi Deng[1,#], Weibin Zhou[1,#], Hongrui Wang[3,4], Qiang Ma[5], Changzhu Li[1,*], Xiongwei Wu[2,3,4,*], Yuping Wu[6,*]

[1]State Key Laboratory of Utilization of Woody Oil Resource of China, Hunan Academy of Forestry, Changsha 410018, Hunan, China.
[2]College of Chemistry and Chemical Engineering, Hunan Normal University, Changsha 410081, Hunan, China.
[3]School of Chemistry and Materials Science, Hunan Agricultural University, Changsha 410128, Hunan, China.
[4]Hunan Engineering Technology Research Center of Vanadium Flow Battery and Energy Storage System, Hunan Province Yinfeng New Energy Co, Ltd., Changsha 410019, Hunan, China.
[5]College of Materials Engineering, Henan International Joint Laboratory of Rare Earth Composite Materials, Henan University of Engineering, Zhengzhou 451191, Henan, China.
[6]Confucius Energy Storage Lab, School of Energy and Environment & Z Energy Storage Center, Southeast University, Nanjing 211189, Jiangsu, China.
[#]Authors contributed equally.

***Correspondence to:** Prof./Dr. Changzhu Li, State Key Laboratory of Utilization of Woody Oil Resource of China, Hunan Academy of Forestry, No. 22 Shaoshan South Road, Changsha 410018, Hunan, China. E-mail: lichangzhu2013@aliyun.com; Prof./Dr. Xiongwei Wu, Hunan Engineering Technology Research Center of Vanadium Flow Battery and Energy Storage System, Hunan Province Yinfeng New Energy Co, Ltd., No. 18 Shawan Road, Changsha 410019, Hunan, China. E-mail: wxw@hunau.edu.cn; Prof./Dr. Yuping Wu, Confucius Energy Storage Lab, School of Energy and Environment & Z Energy Storage Center, Southeast University, No. 2 Southeast University Road, Nanjing 211189, Jiangsu, China. E-mail: wuyp@seu.edu.cn

How to cite this article: Deng, Q.; Zhou, W.; Wang, H.; Ma, Q.; Li, C.; Wu, X.; Wu, Y. Design of a polymer electrolyte membrane for enhanced zinc anode stability in reversible aqueous zinc-ion batteries. *Energy Mater.* **2025**, *5*, 500103. https://dx.doi.org/10.20517/energymater.2024.299

Received: 24 Dec 2024 **First Decision:** 5 Feb 2025 **Revised:** 25 Mar 2025 **Accepted:** 10 Apr 2025 **Published:** 16 May 2025

Academic Editor: Bin Wang **Copy Editor:** Fangling Lan **Production Editor:** Fangling Lan

Abstract

Aqueous zinc-ion batteries (ZIBs) hold great promise for energy storage applications. Nevertheless, the realization of high-capacity ZIBs with extended cycle durability remains a significant scientific challenge, predominantly attributed to two inherent limitations: the uncontrollable dendritic growth and concomitant side reactions. In this study, we present a polymer electrolyte membrane denoted as TAC, which addresses these challenges by enhancing the uniform distribution of zinc ions. By incorporating phenolic hydroxyl groups from tannic acid (TA) onto the surface of cellulose fibers, TAC is synthesized, which not only effectively shields both the front and back surfaces of the zinc anode from corrosive effects of the liquid electrolyte, but also exhibits a high liquid-retention

capacity under pressures up to 5 MPa. Combining density functional theory simulations with experimental investigations, we demonstrate that the phenolic hydroxyl groups from TA actively engage with zinc ions, thereby significantly reducing the desolvation energy during the plating/stripping processes of the zinc anode. The assembled battery utilizing 1% TAC achieves remarkable performance, retaining 83.1% of its discharge capacity after 1,000 cycles at a current density of 5 C. Moreover, it exhibits high reversibility, high coulombic efficiency of 99.9%, and an impressive lifespan exceeding 2,300 h at 0.5 mA cm^{-2}. Furthermore, 1% TAC demonstrates excellent cycling stability across four different electrolyte systems [$ZnSO_4$, $Zn(CF_3SO_3)_2$, $Zn(OAc)_2$, and $ZnCl_2$], highlighting its outstanding compatibility across diverse electrolyte compositions. The exceptional performance of the assembled batteries underscores the efficacy of our design, offering a novel strategy for the development and fabrication of polymer electrolyte membranes tailored for aqueous ZIBs.

Keywords: Aqueous zinc ions batteries, tannic acid, electrolyte, cellulose, zinc anode

INTRODUCTION

The heightened prevalence of environmental pollution and escalating energy consumption have spurred the dynamic advancement of clean and renewable energy technologies. However, the intermittent nature and inherent variability of wind and solar energy have posed obstacles to their seamless integration into electrical infrastructure. Consequently, the storage and conversion of energy necessitate secondary batteries endowed with superior performance characteristics to ensure the consistent delivery of clean power. Among the widely discussed secondary batteries, zinc-ion batteries (ZIBs), utilizing a blend of pure water and zinc salts as electrolytes, have emerged as a promising contender for large-scale energy storage and mobile power applications. This is attributed to their notable features of being low-cost, high-energy, highly safe, and environmentally friendly[1-6]. However, the utilization of ZIBs is significantly impeded by the instability of zinc metal anodes during the plating/stripping process[7], primarily attributable to zinc dendrites, zinc corrosion, and side reactions occurring on the anode[8-10]. Zinc dendrites, characterized by a high Young's modulus, proliferate with cycling, introducing dead zinc metal that extends to the cathode and induces short circuits in the battery. Conversely, pure zinc metal is prone to corrosion when exposed to salt solutions, leading to its degradation and the accumulation of byproducts on the anode surface. This circumstance severely hampers the zinc plating/stripping process and diminishes the cycling lifespan of ZIBs. To address these challenges and enhance the reversibility of the anode in ZIBs, numerous effective strategies have been proposed. These include the incorporation of additives into the electrolyte[5,11,12], the fabrication of semi/all-solid-state electrolytes[13-17], the construction of layered protection around the anodes[10,18,19], the design of intricate anode structures[20-24], and the utilization of polymer electrolytes[25-27]. Among these approaches, the utilization of polymer electrolytes stands out as the simplest and most effective method to enhance the electrochemical performance of ZIBs. Polymer electrolytes offer numerous advantages[28,29], including higher electrolyte-confinement capability[30], superior uniform distribution of ions in solution, easily controlled thickness, broader operating temperatures, and better interface compatibility[28] compared to aqueous electrolytes. Furthermore, owing to their cross-linked structure and functional groups, the electrochemical properties of the polymer can be readily optimized through the design of unique structures, incorporation of functional groups, and combination with other materials[29,31].

In order to mitigate zinc dendrite formation and enhance ion conductivity in ZIBs using optimized polymer electrolytes, researchers have proposed and designed a series of polymer electrolytes. These include poly (ethylene oxide)[32], xanthan gum[33], gelatin[34], polyacrylamide[35], carboxymethyl cellulose sodium[36], and polyvinyl alcohol[37,38]. It is noteworthy that the aforementioned polymer electrolytes have demonstrated excellent electrochemical performance with significant implications. However, the preparation processes are complicated and often yield numerous byproducts. Therefore, there is an urgent need to develop high-

performance ZIBs by utilizing polymer electrolytes based on sustainable materials through easily implementable methods.

Cellulose, a renewable biomaterial composed of nanofibers made of hexose units, possesses exceptional hydrophilicity and moisture retention due to the abundance of hydroxyl groups along its lengthy chains. Additionally, it boasts advantages such as low cost, sustainability, biodegradability, chemical stability, and widespread availability as a natural polymer, rendering it a promising candidate for high-performance electrolytes in ZIB applications[39-43]. However, the pristine cellulose-based electrolytes in ZIBs exhibit poor performance and low capacity during cycling, primarily due to their inability to prevent the formation of zinc dendrites on the anode and the dissolution of cathode materials.

In this study, a polymer electrolyte membrane (TAC) was synthesized by incorporating tannic acid (TA) into cellulose, facilitating the formation of ether bonds and introducing numerous phenolic hydroxyl groups. Compared to pristine cellulose, TAC exhibits enhanced liquid retention capacity, effectively mitigating cathode material dissolution and non-reactive parts corrosion of zinc foil. Moreover, the lower binding energy (E_b) of phenolic hydroxyl groups and zinc ions in TAC, compared to pristine cellulose, significantly inhibits zinc dendrite growth on the anode, resulting in reduced desolvation energy and accelerated uniform zinc ion deposition. These findings were corroborated through thermodynamic calculations and Zn-MnO_2 battery test. Notably, a battery employing 1% TAC demonstrated impressive performance metrics, maintaining a high discharge capacity retention of 83.1% after 1,000 cycles at a current density of 5 C, coupled with exceptional reversible ability (99.9% coulombic efficiency) and prolonged lifespan exceeding 2,300 h at a current density of 0.5 mA cm^{-2}. This innovative design not only provides effective strategies for fabricating high-performance ZIBs but also holds promise for broader applications in secondary batteries. Hence, as depicted in Figure 1A, TAC was synthesized by introducing TA into the cellulose solution. In brief, a homogeneous cellulose solution was blended with TA and reacted in pure water for approximately 30 min. The reaction between cellulose and TA resulted in the formation of a polymer electrolyte membrane, which was subsequently vacuum-filtered to produce a film with abundant phenolic hydroxyl groups distributed on the surface of the fibers. Figure 1B illustrates the schematic diagram for protecting the Zn anode. It is noteworthy that due to the stronger attractive interaction between the phenolic hydroxyl groups in TAC and Zn^{2+}, the flux of zinc ions was effectively and uniformly regulated. Consequently, in the absence of TA, the battery produced vertical zinc dendrites after extended cycling. Conversely, in the presence of TA, zinc deposition and stripping occurred uniformly, resulting in horizontally stacked zinc layers without zinc dendrites.

EXPERIMENTAL

Preparation of TAC: X% (X = 0, 0.5, 1, 3) TAC was prepared as follows: 2 g bacterial cellulose (solid content = 70%, Guilin Qihong Technology Co. Ltd) was dispersed in 100 mL pure water through magnetic stirring for 30 min; then, X g (X = 0, 0.5, 1, 3) TA (98%, Macklin) was dissolved in abovementioned mixture and stirred for 30 min, respectively, which formed TAC films by vacuum filtration. TAC films were dried at 80 °C until constant weight. According to the mass of the TA (X = 0, 0.5, 1, 3), the samples was named as X% (X = 0, 0.5, 1, 3) TAC, respectively.

MnO_2/carbon nanotube (CNT) material was synthesized referencing a previous work with a slight modification[44]; the detail of experiment was as follows: 0.15 g multi-walled CNT (diameter: 5-15 nm, length: 10-30 μm, Nanjing XFNANO Materials Tech Co., Ltd) with hydroxylation was dispersed in 150 mL pure water and 2.03 g $MnSO_4$ (AR grade, Aladdin) was added into the above solution stirring for 30 min. 1.27 g $KMnO_4$ (AR grade, Alfa) was dispersed into 80 mL pure water stirring for 30 min and added into the

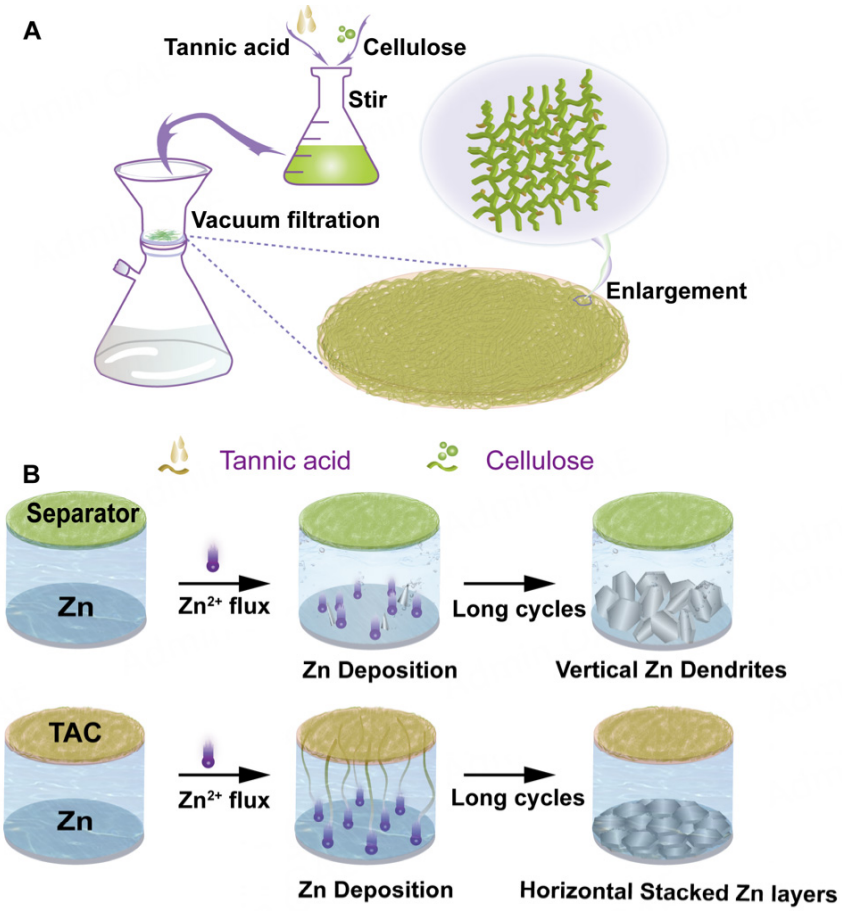

Figure 1. Schematic of (A) the fabrication process of TAC; (B) the protection diagram for Zn anode.

above solution slowly stirring for 10 min. Then, the mixture solution was transferred to an autoclave heating for 12 h at 120 °C and obtained a dark brown powder through filtering and drying.

For preparing cathode electrode, MnO_2/CNT powder, super P carbon black (TIMCAL), and poly(vinylidene fluoride) binder(Arkema) (weight ratio of 7:2:1) were mixed in N-Methylpyrrolidone solvent (99.9%, Aladdin), stirred for 1 h, and coated on a piece of single-walled CNTs paper (Nanjing XFNANO Materials Tech Co., Ltd). Then it was dried in a vacuum at 70 °C and cut into electrodes with a diameter of 9 mm and a mass loading of 0.6-1.5 mg MnO_2. Zinc foil (purity > 99.98%, Alfa) was polished using sandpaper and used as anode.

Characterization: The surface morphology of electrode and TAC materials was revealed using a scanning electron microscope (SEM) (Zeiss Sigma 300). The functional groups and chemical states of TAC materials were investigated by X-ray photoelectron spectroscopy (XPS) (Thermo Scientific K-Alpha) and Fourier transform infrared spectroscopy (FTIR) spectra (Thermo Scientific Nicolet iS5). An electronic universal testing machine (MTS CMT6103) and optical contact angle measuring system (KRUSS DSA100) were utilized to evaluate the mechanical properties and wettability of TAC materials. The thermal curves were performed by simultaneous thermal analyzer (NETZSCH STA 449F5) at 10 °C min^{-1} under nitrogen atmosphere.

Electrochemical measurements: Cyclic voltammetry (CV) curves, linear sweeping voltammetry (LSV), and electrochemical impedance spectroscopy (EIS) were tested using an Admiral potentiostats (Squidstat Plus). The CV and LSV were conducted using polished Zn foil and obtained MnO_2/CNT material corresponding to the counter electrode, the reference electrode, and the work electrode, respectively. Electrochemical properties of Zn-MnO_2 batteries (voltage range of 0.8-1.85 V) and Zn||Zn batteries were tested using CR2032-type coin cells and 2001A battery testing system at 25 °C. Before the X% TAC materials were used as polymer electrolyte membranes, a small amount of 2 M $ZnSO_4$ mixed with 0.1 M $MnSO_4$, 2 M $Zn(CF_3SO_3)_2$ mixed with 0.1 M $Mn(CF_3SO_3)_2$, 2 M $Zn(OAc)_2$, or 2 M $ZnCl_2$ was added into the X% TAC materials. Additionally, except where otherwise stated, all the electrochemical results are gathered using 2 M $ZnSO_4$ mixed with 0.1 M $MnSO_4$ as the electrolyte.

The liquid retention capacity of TAC materials under 5 MPa was determined by

$$\text{Liquid retention capacity (\%)} = (M_1 - M_0)/M_0 \times 100\% \quad (1)$$

where M_0 is the weight of TAC before soaked in the mixture solution of 2 M $ZnSO_4$ + 0.1 M $MnSO_4$. M_1 is the weight of TAC after being soaked in the mixture solution under 5 MPa.

The test of liquid retention rates with 5 MPa: First, 0%, 0.5%, 1%, and 3% TAC were cut into samples with 19 mm diameter and soaked in the liquid electrolyte with 2 M $ZnSO_4$ + 0.1 M $MnSO_4$ for 6 h. The weights of abovementioned polymer electrolytes were recorded and named as M_0 and M_1, where M_0 is the weight of TAC before soaked in the mixture solution of 2 M $ZnSO_4$ + 0.1 M $MnSO_4$. M_1 is the weight of TAC after being soaked in the mixture solution under pressure of 5 MPa. The hollow diameter size of bibulous paper is larger than 19 mm (by 1-2 mm) avoiding the polymer electrolyte contact with bibulous directly.

DFT calculation: The first principal calculation was conducted in the computational chemistry package of Gaussian 16 program[45] based on the density functional theory (DFT). The optimized structures without virtual frequency were acquired with the B3LYP functional[46]. The basis set 6-311+G (d, p)[47] with D3 (BJ)[48] was utilized for C, H and O atoms while the SDD basis set[49,50] with an effective core potential (ECP) was employed for Zn atoms. The impact of the water solvent environment on all the systems was taken into consideration on the basis of the IEFPCM model[51] for structure optimization. The Multiwfn[52-55] and VMD[56] program were utilized in the calculation and analysis of electrostatic potential (ESP) on molecule surface. The binding energies of all systems were calculated under the M06-2X-D3/def2-TZVP[57-59] level and the ECP was also used for Zn atoms. The solvation model density (SMD) model[60] was taken into consideration in the calculation of binding energies. The E_b for system was defined according to

$$E_b = E_{total} - (E_1 + E_2) \quad (2)$$

where E_{total}, E_2, and E_1 stand for the energy for the interaction system, the different substrate materials (0% TAC, 1% TAC), and Zn^{2+}, respectively.

RESULTS AND DISCUSSION

Optical images illustrating TAC concentrations of 0%, 0.5%, 1%, and 3% are shown in Supplementary Figure 1A-D. Relative to the optically clear 0% TAC, the transparency of X% TAC (where X = 0.5, 1, 3) decreased proportionally with increasing TA content. Scanning electron microscopy (SEM) was employed to investigate the microstructure of TAC, revealing a three-dimensional porous network comprising randomly oriented nanofibers of varying diameters, as depicted in Figure 2A-D. While 0% TAC

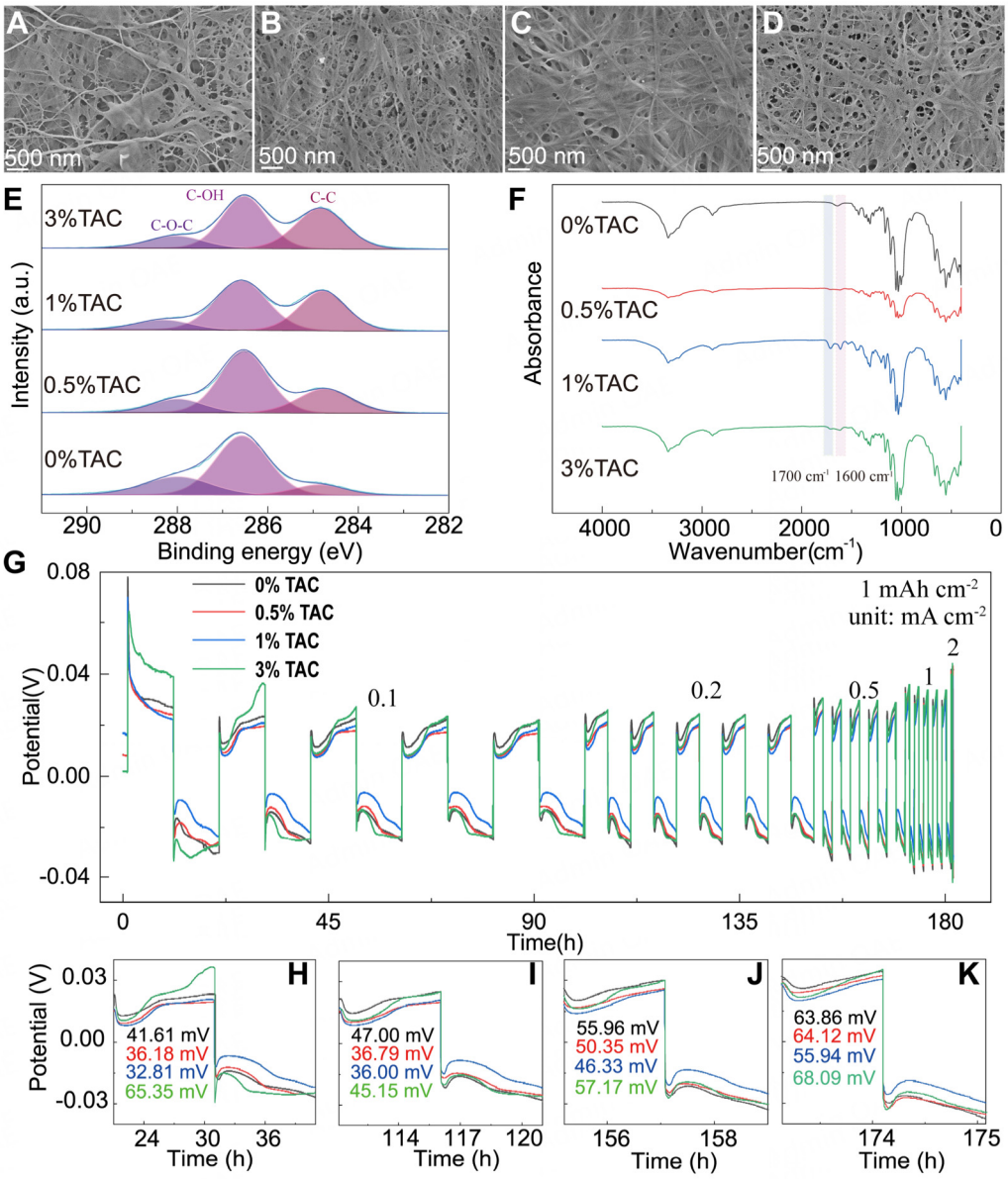

Figure 2. SEM images of (A) 0% TAC, (B) 0.5% TAC, (C) 1% TAC, and (D) 3% TAC; (E) XPS of C 1s of the TAC samples; (F) FTIR spectra of TAC samples; (G) Galvanostatic Zn stripping and plating in a Zn||Zn cell using TAC under different current density (0.1, 0.2, 0.5, 1, and 2 mA cm^{-2}) with 1 mAh cm^{-2} capacity limitation; Potential profiles of Zn/Zn cell under (H) 0.1, (I) 0.2, (J) 0.5, and (K) 1 mA cm^{-2} for a specified time range with a capacity limitation of 1 mAh cm^{-2}.

showed numerous irregular pores, the introduction of TA resulted in composite TAC structures featuring well-defined pores and a dense fiber arrangement. Notably, 1% TAC exhibited fewer pores and tightly interconnected fibers compared to both 0.5% and 3% TAC. This characteristic is advantageous for suppressing the formation of zinc dendrites during the plating/stripping process[61]. XPS was utilized to probe the chemical bonds present on the surface of TAC. Analysis via XPS revealed the presence of various functional groups such as C-C, C-OH, and C-O-C, identified by their respective binding energies of 284.8, 286.5, and 288 eV[62,63], as illustrated in Figure 2E.

Upon the addition of TA, there was an observable increase in the C-O-C content of TAC, suggesting a reaction between TA and the oxygen groups within the cellulose matrix [Supplementary Table 1]. Furthermore, comparison of the infrared spectroscopy (IR) spectrum of 0% TAC with those of 0.5%, 1%, and 3% TAC revealed prominent absorption peaks around ~1,700 and 1,600 cm^{-1}, indicative of C=O and aromatic skeletal vibrations[64,65]. This observation suggests the introduction of TA onto the cellulose surface, as shown in Figure 2F. Interestingly, despite having different TA contact angles (measured at 40.7°, 68.9°, 46.5°, and 35.4°, for 0%, 0.5%, 1%, and 3% TA, respectively, as illustrated in Supplementary Figure 2, all TAC samples demonstrated comparable levels of hydrophilic performance. Supplementary Figure 3A depicts the test results regarding the liquid retention capacity of TAC materials at concentrations of 0%, 0.5%, 1%, and 3% under a pressure of 5 MPa. It is evident that the liquid retention capacity increases with higher TA content, indicating that TA-modified cellulose exhibits enhanced capacity in retaining liquid electrolytes, particularly under elevated pressure conditions, as illustrated in Supplementary Figure 3B. This heightened liquid retention capability serves to shield the zinc foil anode from corrosion by the liquid electrolyte. Notably, during charging and discharging at a current density of 5 C for approximately 36 h, the rear surface of the zinc foil in batteries using 1% TAC appeared notably smoother compared to those employing 0% TAC. The latter exhibited pronounced corrosion with numerous perforations in the non-reactive region, as evidenced in Supplementary Figure 4. To investigate the electrochemical characteristics of the polymer electrolyte membrane containing 0%, 0.5%, 1%, and 3% TAC, as depicted in Figure 2G, galvanostatic zinc plating/stripping processes were conducted within a Zn||Zn cell across various current densities ranging from 0.1 to 2 mA cm^{-2}, with a consistent capacity of 1 mAh cm^{-2}. The Zn||Zn cell incorporating 1% TAC displayed overpotential values of 32.81, 36.00, 46.33, and 55.94 mV at current densities of 0.1, 0.2, 0.5 and 1 mA cm^{-2}, respectively. This outcome suggests that 1% TAC could serve effectively as a polymer electrolyte membrane, enhancing the electrochemical performance of the zinc anode during the plating/stripping process, as delineated in Figure 2H-K. To comprehensively assess the electrochemical attributes of TAC materials, both 0% and 1% TAC were employed as polymer electrolyte membranes in Zn-MnO_2 batteries. Supplementary Figure 5A and B shows the structure and morphology of the positive electrode materials, characterized by small-sized particles (~200 nm) comprising nanotubes intermixed with MnO_2 nanosheets. Additionally, Figure 3A and B illustrates smoother, flatter surface with more uniform and denser fiber structures in 1% TAC compared to 0% TAC. These features are advantageous for mitigating zinc dendrite growth towards the positive electrode, thus averting internal short circuits within the battery[66]. The introduction of 1% TA resulted in the formation of interwoven tortuous nanosized pores within denser fibers, a notable improvement over the 0% TAC shown in Figure 3C and D. This structural modification led to a reduction in pore size. Exothermic data, as shown in Supplementary Figure 5C, and collected via differential scanning calorimetry (DSC), revealed specific peaks at 249, 362, 346 and 352 °C corresponding to pristine cellulose, TA, TA/pristine cellulose composite, and 1% TAC, respectively. Compared to the TA/pristine cellulose composite, the exothermic peak of 1% TAC exhibited reduced intensity, lower density, and narrower peak width, indicative of a reaction between TA and cellulose[67,68].

The electrochemical stability of 0% and 1% TAC was investigated through LSV curves, employing a limited voltage of 2.5 V and a scan rate of 0.1 mV s^{-1}, as shown in Supplementary Figure 5D. It was observed that the current profiles of 0% and 1% TAC in Zn-MnO_2 batteries remained stable below 1.54 and 1.90 V, respectively. This suggests that 1% TAC exhibits superior stability, particularly at higher voltage. Furthermore, the stability and electrochemical performances of TAC materials and both positive and negative electrodes were assessed using EIS and CV, as illustrated in Supplementary Figure 6A-D. Notably, in the context of Zn-MnO_2 batteries, 1% TAC demonstrated enhanced electrochemical stability and interfacial compatibility compared to 0% TAC. To explore the protective role of TAC on the Zn anode, Zinc foils were employed as electrodes in Zn||Zn batteries, utilizing both 0% and 1% TAC with a 2 M $ZnSO_4$ electrolyte. These batteries underwent plating and stripping cycles for 700 h at a current density of

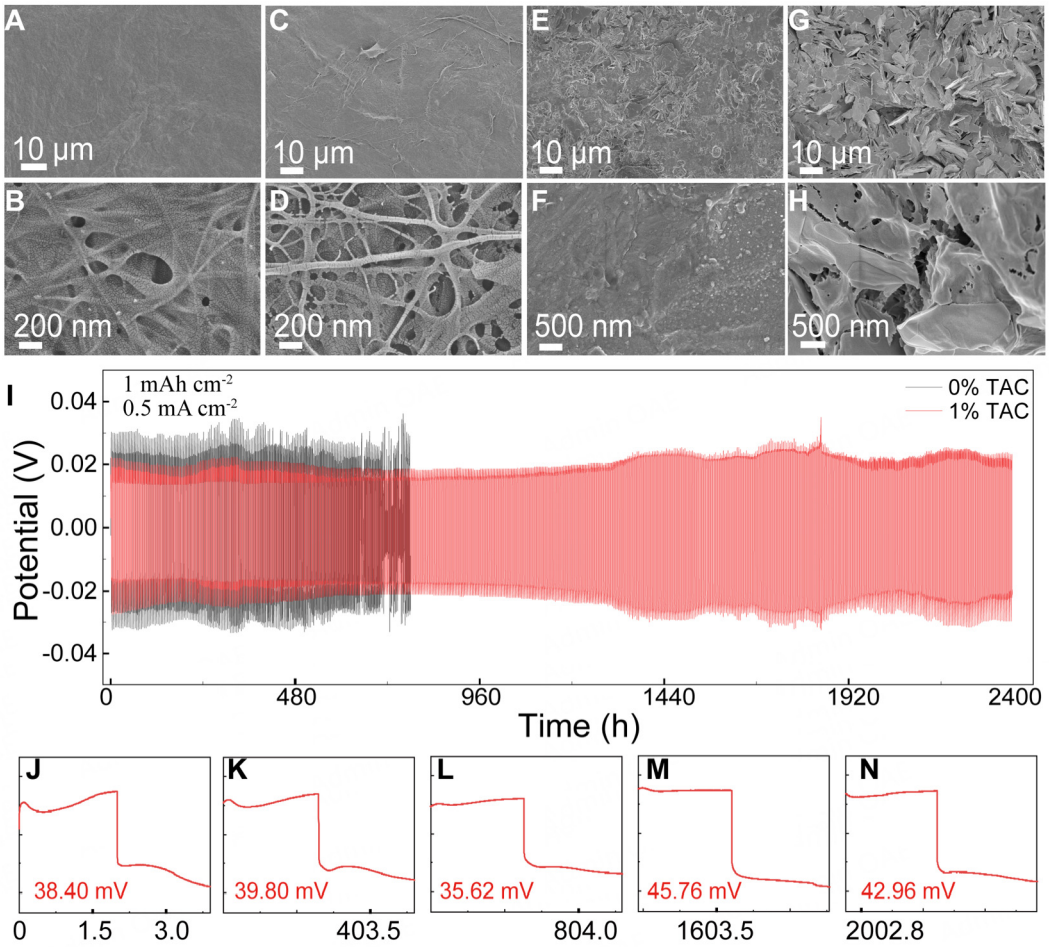

Figure 3. SEM images of (A) 10 μm and (B) 200 nm of 1% TAC, (C) 10 μm and (D) 200 nm of 0% TAC; SEM images of Zn anode in Zn||Zn symmetry cells after 700 h plating/stripping cycles in $ZnSO_4$ using (E) 10 μm and (F) 500 nm of 1% TAC, (G) 10 μm and (H) 500 nm of 0% TAC at 0.5 mA cm^{-2}; (I) Galvanostatic Zn stripping and plating in a Zn||Zn cell using TAC with 2 M $ZnSO_4$ as the electrolyte under current density of 0.5 mA cm^{-2} with 1 mAh cm^{-2} capacity limitation; Potential profiles of Zn||Zn cell plating/stripping cycles using 1% TAC at (J) the first, (K) the 100th, (L) 200th, (M) 400th, (N) 500th with 1 mAh cm^{-2} capacity limitation.

0.5 mA cm^{-2}. The zinc foils displayed notable differences in anode surface morphology, clearly observed in the SEM images shown in Figure 3E-H. In comparison to the pristine zinc foil [Supplementary Figure 7], the anode foil from the battery that used 0% TAC exhibited a coarse surface with abundant flake-like zinc dendrites, as shown in Figure 3G. Furthermore, these dendrites featured cracking and irregular protuberances, leading to discontinuous morphology as shown in Figure 3H, indicating potential short-circuiting and premature battery failure due to dendrite growth with cycling. In contrast, that utilizing 1% TAC resulted a relatively smooth surface with densely packed nanostructures, as shown in Figure 3E and F, after approximately 700 h of plating/stripping process. To explore the cyclability of zinc electrodes containing different concentration of TAC mixed with $ZnSO_4$ at a current density of 0.5 mA cm^{-2}, electrochemical performance assessments were carried out using Zn||Zn symmetric cells. Results depicted in Figure 3I illustrate that after 700 h of cycling, the polarization voltages of cells utilizing 1% TAC were notably lower compared to those employing 0% TAC. This discrepancy was attributed to the side reaction occurring on the surface of the zinc foil in 0% TAC-containing cells, leading to the formation and accumulation of zinc dendrites with the increased cycles, as shown in Figure 3G. Upon cycling for 700 h at a limited capacity of 1 mAh cm^{-2}, the battery using 0% TAC showed an erratic polarization voltage behavior

and eventual short circuits. Conversely, the battery using 1% TAC exhibited comparatively stable polarization voltage profiles and sustained functionality for over 2,300 h at a current density of 0.5 mA cm^{-2}. To monitor the evolution of polarization voltages over cycling, potential profiles of Zn||Zn cells utilizing 1% TAC were recorded at a limited capacity of 1 mAh cm^{-2}. Notably, the potentials observed after the first, 100th, 200th, 400th, and 500th cycles were 38.40, 39.80, 35.62, 45.76, and 42.96 mV, respectively [Figure 3J-N], indicating sustained stability of the zinc foil anode during the plating/stripping processes. Furthermore, to elucidate the intrinsic advantages of 1% TAC over 0% TAC, the influence of cellulosic hydroxyl and phenolic hydroxyl groups on the solvation structure of zinc ions was investigated via DFT calculations, as shown in Supplementary Figure 8. Comparative analysis between 1% TAC and 0% TAC is presented in Figure 4. Figure 4A shows the typical electrochemical reactions of Zn^{2+} in the batteries that used 0% TAC or 1% TAC as a polymer electrolyte membrane on the interface of the zinc foil anode. Zn^{2+} interacted with cellulose modified with or without TA. As shown in Supplementary Figure 9, the E_b of 0% TAC-Zn^{2+} and 1% TAC-Zn^{2+} was -0.2898 and -0.5713 eV, respectively. It was established that the participation of phenolic hydroxyl from TAC is conducive to the desolvation and deposition of zinc ions on the zinc foil anode[69,70]. Figure 4B displayed energy gap between the highest occupied molecular orbital (HOMO) and the lowest unoccupied molecular orbital (LUMO) of 1% TAC and 0% TAC. Obviously, 1% TAC exhibited a lower energy gap than 0% TAC, which implied better electrical conductivity of 1% TAC than 0% TAC[71,72], in accordance with the abovementioned conclusion from the summary energies. Figure 4C and D showed the ESP distribution on the Van der Waals surface of 1% TAC and 0% TAC, respectively. In comparison to larger pink and white regions with positive ESP and reactive sites of hydroxyl groups from 0% TAC, there were larger light blue and gentian blue regions with negative ESP of phenolic hydroxyl from 1% TAC, which provides more abundant active sites to induce the deposition and stripping of Zn^{2+}[70,73].

Hence, the maxima ESP value of 1% TAC with Zn^{2+} was reduced to 395.1561 kcal mol^{-1}, which was lower than that of 0% TAC with Zn^{2+} (440.0305 kcal mol^{-1}), as shown in Supplementary Figure 10. Therefore, in comparison with 0% TAC, the easier interaction and stronger attraction interaction between 1% TAC and Zn^{2+} indicated that the desolvation process of Zn^{2+} with 1% TAC was easier than that with 0% TAC. Less energy was consumed during the process when zinc ions left the electrolyte to move to the interface of the anode electrode, which made the reaction process easier and boosted the uniform distribution of zinc ions on the zinc foil electrode. As a result of the weaker attraction interaction between 0% TAC and Zn^{2+}, zinc ions were nonuniformly distributed on the surface of the anode electrode and a large number of dendrites were found, as shown in Figure 4A. On the other hand, 1% TAC possessed abundant hydroxyl and π-π stacking that exhibited high interaction with H_2O molecules, which ensured excellent liquid electrolyte retention of the 1% TAC at 5 MPa. In addition, in order to assess the compatibility of the TAC with different electrolytes, galvanostatic Zn stripping and plating in a Zn||Zn cell using TAC was conducted in various electrolytes, as shown in Figure 5. After long cycles of the Zn foil with 1% TAC in $Zn(CF_3SO_3)_2$ as shown in Figure 5A, abundant regular bulks composed of stacked flakes can be observed. while in Figure 5B from the battery using 0% TAC, amounts of vertically stacked flakes interlaced each other and a mass of tiny particles dispersed on the surface, indicating zinc dendrites and other byproducts from side reactions during the cycles. Similarly, from the Zn anode with 1% TAC in $Zn(OAc)_2$ shown in Figure 5C, horizontally stacked flakes in small size interweaved and stayed close together; on the contrary from 0% TAC in Figure 5D, massive vertical bulks connected with each other, which is the same as the one from $ZnCl_2$ in Figure 5F. In Figure 5E from 1% TAC in $ZnCl_2$, irregular flakes horizontally stacked and formed multi-hierarchy structure. The above results demonstrated that 1% TAC induced uniform distribution of Zn ions, which effectively inhibited the growth of zinc dendrites.

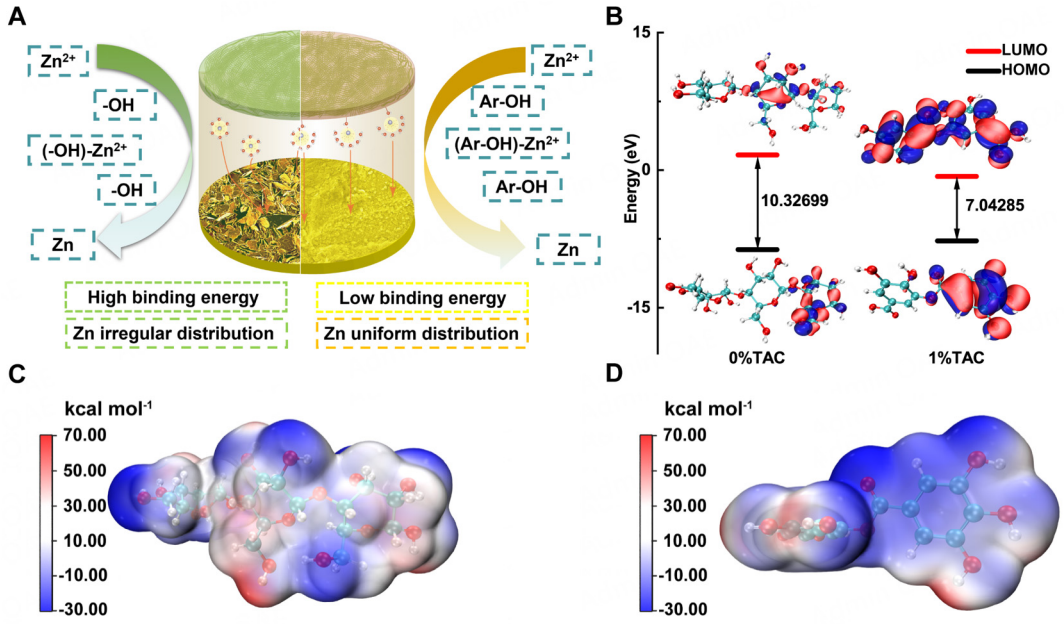

Figure 4. (A) Schematic of Zn^{2+} plating/stripping process by using 0% TAC or 1% TAC; (B) LUMO and HOMO gap comparison between 1% TAC and 0% TAC; electrostatic potential (ESP) distribution on the Van der Waals surface of (C) 0% TAC and (D) 1% TAC.

Hence, the cycle performance of 1% TAC is prior to that of 0% TAC, which was displayed in Figure 5G for $Zn(CF_3SO_3)_2$ and Figure 5H for $Zn(OAc)_2$. Concretely, when in $Zn(OAc)_2$ at 2 mA cm^{-2}, 1% TAC nearly stably cycles for 1,200 h while the battery using 0% TAC shot-circuited within 100 h; when used in $Zn(CF_3SO_3)_2$ at 0.5 mA cm^{-2}, 1% TAC consistently steadily work for 2,800 h without degradation while 0% TAC failed in short time. Besides, when utilized in $ZnCl_2$ at 0.5 mA cm^{-2} as shown in Supplementary Figure 11, 1% TAC performed steadily for 420 h; inversely, the battery using 0% TAC failed within 75 h. In short, 1% TAC with outstanding performances and compatibility could be used as a polymer electrolyte membrane in different electrolytes for ZIBs.

In addition, the CV curves of the Zn-MnO_2 batteries that used 0% TAC or 1% TAC were investigated, as shown in Figure 6A. Both CV profiles presented similar redox reaction pairs, indicating that 1% TAC did not influence the intercalation/deintercalation process of Zn^{2+}. To study the electrochemical properties of the TAC, CNT paper with MnO_2, 0% TAC or 1% TAC, and zinc foil, were used as the positive electrode, polymer electrolyte membrane, and negative electrode assembled in Zn-MnO_2 batteries, respectively. To investigate the adaptability of 1% TAC, the electrochemical performance of the assembled battery was investigated in $ZnSO_4$, as shown in Figure 6B-D and $Zn(CF_3SO_3)_2$, as shown in Figure 6E-G, as the matrix of the aqueous electrolyte, respectively. As shown in Figure 6B, the battery using 1% TAC displayed a higher rate capability than that using 0% TAC. This was because 1% TAC possessed abundant phenolic hydroxyls, which modified the solvation environment of Zn^{2+} ions, weakened the solvation-free energy, and ultimately lowered the reaction barrier for the deposition and insertion of zinc ions[74]. The Zn-MnO_2 battery using 1% TAC with $ZnSO_4$ exhibited excellent discharge capacities of 288.1, 254.7, 221.5, 202.0, 188.3, and 178.1 mAh g^{-1}, which were higher than those used the 0% TAC at current densities of 0.5, 1, 2, 3, 4, and 5 C. This was due to the lower solvation-free energy and the faster redox reactions of the positive material. Moreover, the coulomb efficiencies of 1% TAC and 0% TAC approached 99.9% at various current densities. When the assembled batteries were operated at a current density of 1 C, the battery using 1% TAC with $ZnSO_4$ exhibited a higher discharge capacity retention of 92.60% and a higher capacity of 33.33% after 100

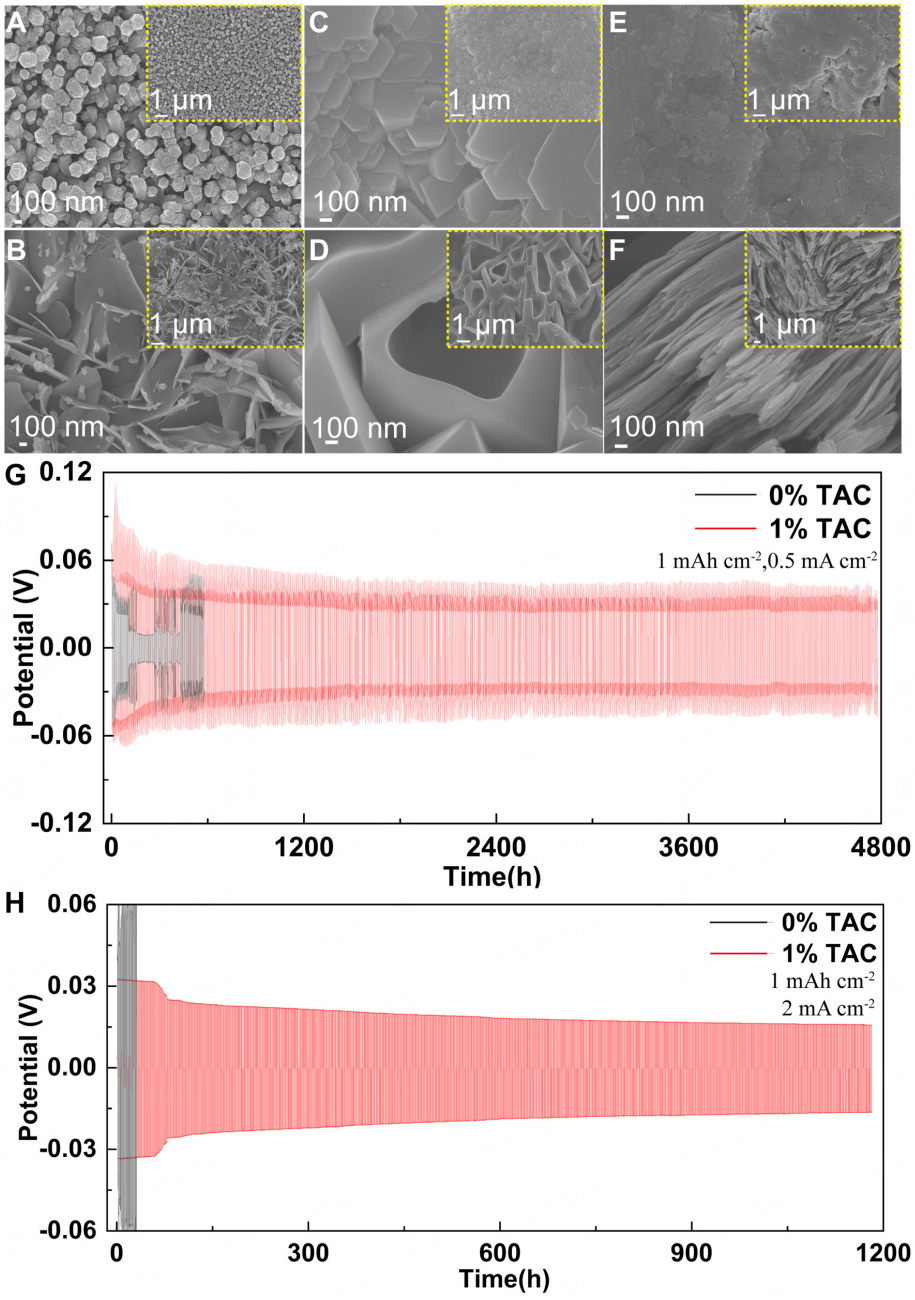

Figure 5. SEM images of Zn anode in Zn|| Zn cells after long cycles in different electrolytes: (A) 1% TAC and (B) 0% TAC in $Zn(CF_3SO_3)_2$, (C) 1% TAC and (D) 0% TAC in $Zn(OAc)_2$, and (E) 1% TAC and (F) 0% TAC in $ZnCl_2$; Galvanostatic Zn stripping and plating in a Zn||Zn cell using TAC with 1 mAh cm^{-2} capacity limitation in the electrolyte of (G) $Zn(CF_3SO_3)_2$ under current density of 0.5 mA cm^{-2}, and (H) $Zn(OAc)_2$ under current density of 2 mA cm^{-2}.

cycles in comparison to that using 0% TAC [Figure 6C]. When the current rate was increased to 5 C, the cyclability of the Zn-MnO_2 battery was investigated using 1% TAC with $ZnSO_4$, as shown in Figure 6D. The first-cycle discharge capacity of the battery using 1% TAC was 178.4 mAh g^{-1} which thereafter changed to 148.3 mAh g^{-1} after 1,000 cycles. Thus, this battery exhibited a high retention capacity of 83.1% at a large current density of 5 C. The coulombic efficiency of the battery using 1% TAC reached 99.9% during 1,000 cycles, which was attributed to the strong inhibitory effect of the 1% TAC on the side reaction and the

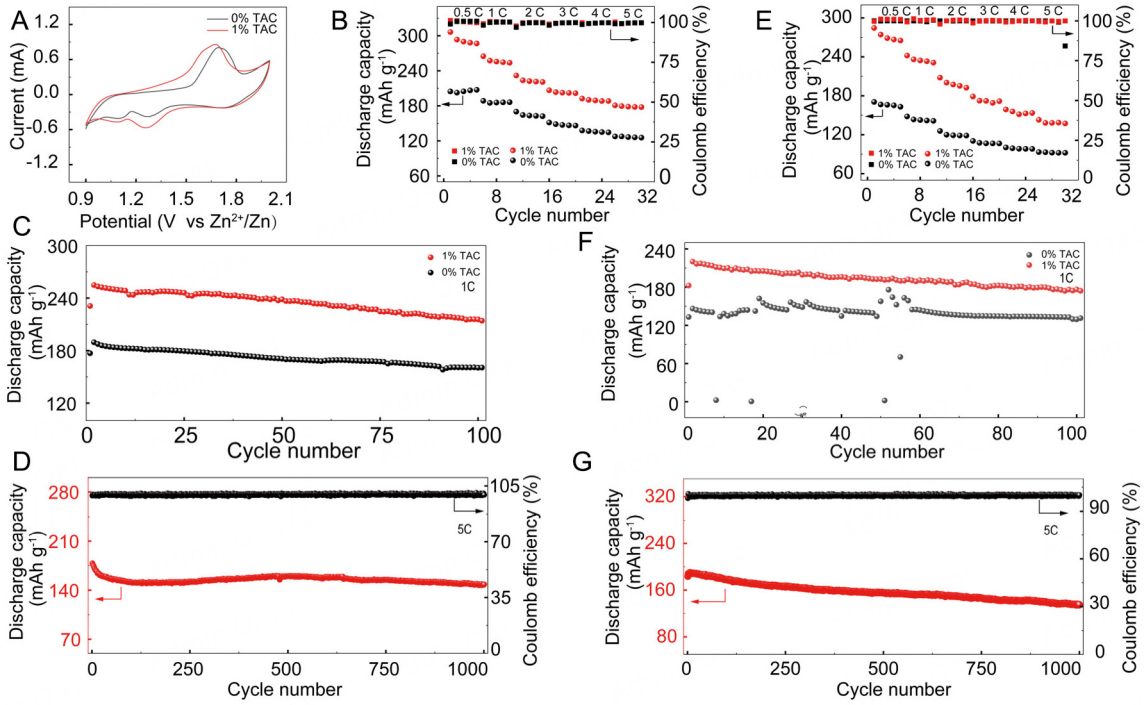

Figure 6. (A) CV curves of 0% TAC and 1% TAC at a scan rate of 1 mV s^{-1}; discharge capacity and the corresponding coulombic efficiency of the battery using $ZnSO_4$ at (B) different current densities, (C) 1 C, (D) 5 C and using 2 M $Zn(CF_3SO_3)_2$ as the electrolyte at (E) different current densities, (F) 1 C, (G) 5 C, respectively.

formation of zinc dendrites. When evaluating the applicability of 1% TAC in different electrolytes, the assembled battery using 1% TAC with $Zn(CF_3SO_3)_2$ exhibited a high discharge capacity of 265.2 mAh g^{-1} at a rate of 0.5 C, as shown in Figure 6E. When the current rate was raised to 1, 2, 3, 4, and 5 C, discharge capacities of 231.1, 192.4, 171.6, 153.5, and 137.4 mAh g^{-1}, could be maintained, respectively. However, the Zn-MnO_2 battery using 0% TAC exhibited discharge capacities of 163.1, 141.4, 118.7, 106.6, 98.2, and 92.1 mAh g^{-1} at current densities of 0.5, 1, 2, 3, 4, and 5 C, respectively, confirming that modifying cellulose with TA could increase the capacity of batteries significantly. The cyclability of Zn-MnO_2 batteries using 0% TAC and 1% TAC were investigated at 1 C for 100 cycles; after 100 cycles, the charge capacity of 1% TAC and 0% TAC with $Zn(CF_3SO_3)_2$ were 174.2 and 131.3 mAh g^{-1}, respectively. Moreover, the discharge capacity of the Zn-MnO_2 battery using 0% TAC with Zn $(CF_3SO_3)_2$ exhibited sharp fluctuations at a current density of 1 C within the first 100 cycles as shown in Figure 6F, which was attributed to the side reactions resulting from the reaction-free electrolyte. To investigate the lifespan of the battery using 1% TAC with $Zn(CF_3SO_3)_2$, the battery was tested at a current density of 5 C for 1,000 cycles, as shown in Figure 6G. The discharge capacity retention maintained at 73.7% and the coulombic efficiency approached 99.9% after 1000 cycles. Thus, the battery using 1% TAC with $ZnSO_4$, or $Zn(CF_3SO_3)_2$ exhibited high capability rates and long-life cyclability, which were ascribed to the outstanding adaptability of 1% TAC to different liquid electrolyte components.

CONCLUSIONS

By regulating cellulose with TA, we obtained a polymer electrolyte membrane of 1% TAC, which possessed a three-dimensional porous network and dense structure with abundant phenolic hydroxyls. Additionally, the 1% TAC delivered a high liquid retention rate at 5 MPa and protected both the front and back surfaces of the zinc foil from corrosion by the electrolyte. Supported by the excellent electrochemical properties

mentioned above and simulation calculations, this strategy has proven to be an efficient way to reduce the hydroxyl groups on the surface of cellulose and increase the quantity of phenolic hydroxyl groups, which suppressed the reaction of the polymer electrolyte and Zn^{2+}, and subsequently demonstrated a lower desolvation energy during the plating/stripping process of Zn^{2+} as well as a lower overpotential. Remarkably, these advantages were beneficial to the uniform distribution of Zn^{2+} on the surface of the anode, the alleviated zinc dendrite, and the prolonged life of the Zn-MnO_2 battery. This novel method has been demonstrated to be an effective strategy for the design and fabrication of high-performance polymer electrolyte membranes for ZIBs, and offers a viable path to assemble other batteries with excellent performance.

DECLARATIONS

Authors' contributions

Writing-original draft, data curation, formal analysis, methodology, investigation, funding acquisition: Deng, Q.
Validation, visualization: Zhou, W.
Data curation, resources: Wang, H.
Formal analysis, investigation: Ma, Q.
Project administration, funding acquisition, software conceptualization: Li, C.
Project administration, supervision, methodology: Wu, X.
Project administration, data curation, writing-review & editing: Wu, Y.

Availability of data and materials

The data supporting our work can be found in the Supplementary Materials.

Financial support and sponsorship

This work was financially supported by the National Natural Science Foundation of China (Grant No. 52103053), Outstanding Youth Fund of Hunan Provincial Forestry Bureau (XLK202448), Huxiang Young Talents of Hunan Province (Grant No. 2022RC1004), Natural Science Foundation of Henan (Grant No. 232300420404), Special Project for Forestry Science and Technology Innovation of Hunan Province (Grant No. XLKY202205), the Innovation Demonstration Project of Chenzhou City (Grant No.2022sfq53), Major Science and Technology Innovation Platform Project (Grant No. 2022PT1004) and State Key Laboratory Open Research Project (Grant No. GZKF202219).

Conflict of Interest

Prof. Wu, Y. serves as the Editor-in-Chief of *Energy Materials*, and Prof. Wu, X. is a member of the journal's Editorial Board. However, neither Wu, Y. nor Wu, X. participated in any editorial decisions, including reviewer selection, manuscript handling, or final evaluations related to this work, while the other authors have declared that they have no conflicts of interest.

Ethical approval and consent to participate

Not applicable.

Consent for publication

Not applicable.

REFERENCES

1. Liu, S.; Zhang, R.; Wang, C.; et al. Zinc ion batteries: bridging the gap from academia to industry for grid-scale energy storage. *Angew. Chem. Int. Ed.* **2024**, *63*, e202400045. DOI
2. Luo, C.; Lei, H.; Xiao, Y.; et al. Recent development in addressing challenges and implementing strategies for manganese dioxide cathodes in aqueous zinc ion batteries. *Energy. Mater.* **2024**, *4*, 400036. DOI
3. Li, J.; Liang, H. Organic cathode materials for aqueous zinc-organic batteries. *Energy. Mater.* **2024**, *4*, 400033. DOI
4. Cui, Y.; Ding, Y.; Guo, L.; et al. Ultra-long $Zn_3V_2O_7(OH)_2·2H_2O$ nanowires grown on carbon cloth as cathode material for aqueous zinc-ion batteries. *Energy. Mater.* **2023**, *3*, 300023. DOI
5. Miao, L.; Guo, Z.; Jiao, L. Insights into the design of mildly acidic aqueous electrolytes for improved stability of Zn anode performance in zinc-ion batteries. *Energy. Mater.* **2023**, *3*, 300014. DOI
6. Han, M.; Chen, D.; Lu, Q.; Fang, G. Aqueous rechargeable Zn-iodine batteries: issues, strategies and perspectives. *Small* **2024**, *20*, e2310293. DOI
7. Li, G.; Sun, L.; Zhang, S.; et al. Developing cathode materials for aqueous zinc ion batteries: challenges and practical prospects. *Adv. Funct. Mater.* **2024**, *34*, 2301291. DOI
8. Ma, Q.; Ma, A.; Lv, S.; et al. Regulating zinc ion transport behavior and solvated structure towards stable aqueous Zn metal batteries. *J. Energy. Chem.* **2024**, *93*, 609-26. DOI
9. Qian, Y.; Chen, L. Interfacial engineering of manganese-based oxides for aqueous zinc-ion batteries: Advances, mechanisms, challenges and perspectives. *J. Energy. Chem.* **2024**, *99*, 553-79. DOI
10. Guo, Y.; Liu, C.; Xu, L.; et al. A cigarette filter-derived nitrogen-doped carbon nanoparticle coating layer for stable Zn-ion battery anodes. *Energy. Mater.* **2022**, *2*, 200032. DOI
11. Zhu, Q.; Sun, G.; Qiao, S.; et al. Selective shielding of the (002) plane enabling vertically oriented zinc plating for dendrite-free zinc anode. *Adv. Mater.* **2024**, *36*, e2308577. DOI
12. Yuan, Y.; Pu, S. D.; Pérez-Osorio, M. A.; et al. Diagnosing the electrostatic shielding mechanism for dendrite suppression in aqueous zinc batteries. *Adv. Mater.* **2024**, *36*, e2307708. DOI
13. Tu, W.; Liang, S.; Song, L.; Wang, X.; Ji, G.; Xu, J. Nanoengineered functional cellulose ionic conductor toward high- performance all-solid-state zinc-ion battery. *Adv. Funct. Mater.* **2024**, *34*, 2316137. DOI
14. Ge, H.; Xie, X.; Xie, X.; et al. Critical challenges and solutions: quasi-solid-state electrolytes for zinc-based batteries. *Energy. Environ. Sci.* **2024**, *17*, 3270-306. DOI
15. Zhang, B.; Cai, X.; Li, J.; et al. Biocompatible and stable quasi-solid-state zinc-ion batteries for real-time responsive wireless wearable electronics. *Energy. Environ. Sci.* **2024**, *17*, 3878-87. DOI
16. Liu, C.; Xu, W.; Zhang, L.; et al. Electrochemical hydrophobic tri-layer interface rendered mechanically graded solid electrolyte interface for stable zinc metal anode. *Angew. Chem. Int. Ed.* **2024**, *63*, e202318063. DOI
17. Cui, Y.; Chen, W.; Xin, W.; et al. Gradient quasi-solid electrolyte enables selective and fast ion transport for robust aqueous zinc-ion batteries. *Adv. Mater.* **2024**, *36*, e2308639. DOI
18. Wang, J.; Peng, J.; Huang, W.; et al. Enabling stable Zn anode with PVDF/CNTs nanocomposites protective layer toward high-performance aqueous zinc-ion batteries. *Adv. Funct. Mater.* **2024**, *34*, 2316083. DOI
19. Lee, Y.; Jeoun, Y.; Kim, J. H.; et al. Selective ion transport layer for stable aqueous zinc-ion batteries. *Adv. Funct. Mater.* **2024**, *34*, 2310884. DOI
20. Liu, Z.; Guo, Z.; Fan, L.; et al. Construct robust epitaxial growth of (101) textured zinc metal anode for long life and high capacity in mild aqueous zinc-ion batteries. *Adv. Mater.* **2024**, *36*, e2305988. DOI
21. Wu, T.; Hu, C.; Zhang, Q.; et al. Helmholtz plane reconfiguration enables robust zinc metal anode in aqueous zinc-ion batteries. *Adv. Funct. Mater.* **2024**, *34*, 2315716. DOI
22. Al-Abbasi, M.; Zhao, Y.; He, H.; et al. Challenges and protective strategies on zinc anode toward practical aqueous zinc-ion batteries. *Carbon. Neutral.* **2024**, *3*, 108-41. DOI
23. Wang, Z.; Zhou, D.; Zhou, Z.; et al. Synergistic effect of 3D elastomer/super-ionic conductor hybrid fiber networks enables zinc anode protection for aqueous zinc-ion batteries. *Adv. Funct. Mater.* **2024**, *34*, 2313371. DOI
24. Zhu, Y.; Liang, G.; Cui, X.; et al. Engineering hosts for Zn anodes in aqueous Zn-ion batteries. *Energy. Environ. Sci.* **2024**, *17*, 369-85. DOI
25. Yan, K.; Fan, Y.; Hu, F.; et al. A "polymer-in-salt" solid electrolyte enabled by fast phase transition route for stable Zn batteries. *Adv. Funct. Mater.* **2024**, *34*, 2307740. DOI
26. Li, Y.; Yang, X.; He, Y.; et al. A novel ultrathin multiple-kinetics-enhanced polymer electrolyte editing enabled wide-temperature fast-charging solid-state zinc metal batteries. *Adv. Funct. Mater.* **2024**, *34*, 2307736. DOI
27. Ji, S.; Luo, H.; Qin, S.; et al. Component fluctuation modulated gelation effect enable temperature adaptability in zinc-ion batteries. *Adv. Energy. Mater.* **2024**, *14*, 2400063. DOI
28. Wang, Y.; Li, Q.; Hong, H.; et al. Lean-water hydrogel electrolyte for zinc ion batteries. *Nat. Commun.* **2023**, *14*, 3890. DOI PubMed PMC
29. Qi, R.; Tang, W.; Shi, Y.; et al. Gel polymer electrolyte toward large-scale application of aqueous zinc batteries. *Adv. Funct. Mater.* **2023**, *33*, 2306052. DOI
30. He, Q.; Chang, Z.; Zhong, Y.; et al. Highly entangled hydrogel enables stable zinc metal batteries via interfacial confinement effect.

ACS. Energy. Lett. **2023**, *8*, 5253-63. DOI

31. Yan, Y.; Duan, S.; Liu, B.; et al. Tough hydrogel electrolytes for anti-freezing zinc-ion batteries. *Adv. Mater.* **2023**, *35*, e2211673. DOI
32. Chinnakutti, K. K.; Treerittiwittaya, W.; Gao, H.; Tapia-Ruiz, N.; Kidkhunthod, P.; Kasemchainan, J. Solid-state Zn-ion batteries using composite cellulose polyethylene oxide materials-Illustration of reaction and capacity fading mechanisms. *Polymer* **2024**, *299*, 126949. DOI
33. Chen, Y.; Zhao, J.; Wang, Y. Quasi-solid-state zinc ion rechargeable batteries for subzero temperature applications. *ACS. Appl. Energy. Mater.* **2020**, *3*, 9058-65. DOI
34. Yang, Z.; Zhang, Q.; Wu, T.; et al. Thermally healable electrolyte-electrode interface for sustainable quasi-solid zinc-ion batteries. *Angew. Chem. Int. Ed.* **2024**, *63*, e202317457. DOI
35. Wang, N.; Liu, H.; Sun, M.; et al. Achieving wide-temperature-range sustainable zinc-ion batteries via magnesium-doped cathodes and gel electrolytes. *ACS. Sustain. Chem. Eng.* **2024**, *12*, 3527-37. DOI
36. Xu, L.; Meng, T.; Zheng, X.; et al. Nanocellulose-carboxymethylcellulose electrolyte for stable, high-rate zinc-ion batteries. *Adv. Funct. Mater.* **2023**, *33*, 2302098. DOI
37. Li, W.; Wang, Y.; Liu, R.; Chen, W.; Zhang, H.; Zhang, Z. Gel polymer-based composite solid-state electrolyte for long-cycle-life rechargeable zinc-air batteries. *ACS. Sustain. Chem. Eng.* **2023**, *11*, 3732-9. DOI
38. Ma, R.; Xu, Z.; Wang, X. Polymer hydrogel electrolytes for flexible and multifunctional zinc-ion batteries and capacitors. *Energy. Environ. Mater.* **2023**, *6*, e12464. DOI
39. Yang, L.; Fu, Y.; Liu, H.; Nie, Q.; Zhang, M.; Shen, Z. Investigating the zinc deposition behavior in aqueous zinc-ion batteries with PEG/cellulose/$ZnCl_2$ water-in-salt electrolytes via a homemade visualized three-electrode tubular cell. *ACS. Sustain. Chem. Eng.* **2023**, *11*, 10311-23. DOI
40. Li, Y.; Yang, S.; You, Y.; et al. Cellulose nanocrystals built multiscale hydrogel electrolyte for highly reversible all-flexible zinc ion batteries. *Chem. Eng. J.* **2024**, *496*, 154357. DOI
41. Lim, G. J. H.; Koh, J. J.; Chan, K. K.; et al. Amorphous cellulose electrolyte for long life and mechanically robust aqueous structural batteries. *Adv. Funct. Mater.* **2024**, *34*, 2313531. DOI
42. Han, X.; Chen, L.; Yanilmaz, M.; et al. From nature, requite to nature: bio-based cellulose and its derivatives for construction of green zinc batteries. *Chem. Eng. J.* **2023**, *454*, 140311. DOI
43. Zhang, H.; Gan, X.; Yan, Y.; Zhou, J. A sustainable dual cross-linked cellulose hydrogel electrolyte for high-performance zinc-metal batteries. *Nanomicro. Lett.* **2024**, *16*, 106. DOI PubMed PMC
44. Li, H.; Han, C.; Huang, Y.; et al. An extremely safe and wearable solid-state zinc ion battery based on a hierarchical structured polymer electrolyte. *Energy. Environ. Sci.* **2018**, *11*, 941-51. DOI
45. Gaussian 16 Rev. C.01/C.02 release notes. Available from: https://gaussian.com/relnotes/ [Last accessed on 16 May 2025]
46. Stephens, P. J.; Devlin, F. J.; Chabalowski, C. F.; Frisch, M. J. Ab initio calculation of vibrational absorption and circular dichroism spectra using density functional force fields. *J. Phys. Chem.* **1994**, *98*, 11623-7. DOI
47. Krishnan, R.; Binkley, J. S.; Seeger, R.; Pople, J. A. Self-consistent molecular orbital methods. XX. A basis set for correlated wave functions. *J. Chem. Phys.* **1980**, *72*, 650-4. DOI
48. Grimme, S.; Ehrlich, S.; Goerigk, L. Effect of the damping function in dispersion corrected density functional theory. *J. Comput. Chem.* **2011**, *32*, 1456-65. DOI PubMed
49. Dolg, M.; Wedig, U.; Stoll, H.; Preuss, H. Energy-adjusted *ab initio* pseudopotentials for the first row transition elements. *J. Chem. Phys.* **1987**, *86*, 866-72. DOI
50. Pritchard, B. P.; Altarawy, D.; Didier, B.; Gibson, T. D.; Windus, T. L. New basis set exchange: an open, up-to-date resource for the molecular sciences community. *J. Chem. Inf. Model.* **2019**, *59*, 4814-20. DOI PubMed
51. Tomasi, J.; Mennucci, B.; Cammi, R. Quantum mechanical continuum solvation models. *Chem. Rev.* **2005**, *105*, 2999-3093. DOI PubMed
52. Lu, T.; Chen, F. Multiwfn: a multifunctional wavefunction analyzer. *J. Comput. Chem.* **2012**, *33*, 580-92. DOI
53. Lu, T.; Manzetti, S. Wavefunction and reactivity study of benzo[a]pyrene diol epoxide and its enantiomeric forms. *Struct. Chem.* **2014**, *25*, 1521-33. DOI
54. Lu, T.; Chen, F. Quantitative analysis of molecular surface based on improved Marching Tetrahedra algorithm. *J. Mol. Graph. Model.* **2012**, *38*, 314-23. DOI
55. Zhang, J.; Lu, T. Efficient evaluation of electrostatic potential with computerized optimized code. *Phys. Chem. Chem. Phys.* **2021**, *23*, 20323-8. DOI
56. Humphrey, W.; Dalke, A.; Schulten, K. VMD: visual molecular dynamics. *J. Mol. Graph.* **1996**, *14*, 33-8. DOI PubMed
57. Grimme, S.; Antony, J.; Ehrlich, S.; Krieg, H. A consistent and accurate ab initio parametrization of density functional dispersion correction (DFT-D) for the 94 elements H-Pu. *J. Chem. Phys.* **2010**, *132*, 154104. DOI PubMed
58. Zhao, Y.; Truhlar, D. G. The M06 suite of density functionals for main group thermochemistry, thermochemical kinetics, noncovalent interactions, excited states, and transition elements: two new functionals and systematic testing of four M06-class functionals and 12 other functionals. *Theor. Chem. Account.* **2008**, *120*, 215-41. DOI
59. Weigend, F.; Ahlrichs, R. Balanced basis sets of split valence, triple zeta valence and quadruple zeta valence quality for H to Rn: Design and assessment of accuracy. *Phys. Chem. Chem. Phys.* **2005**, *7*, 3297-305. DOI PubMed

60. Marenich, A. V.; Cramer, C. J.; Truhlar, D. G. Universal solvation model based on solute electron density and on a continuum model of the solvent defined by the bulk dielectric constant and atomic surface tensions. *J. Phys. Chem. B.* **2009**, *113*, 6378-96. DOI PubMed
61. Lv, D.; Chai, J.; Wang, P.; et al. Pure cellulose lithium-ion battery separator with tunable pore size and improved working stability by cellulose nanofibrils. *Carbohydr. Polym.* **2021**, *251*, 116975. DOI
62. Chen, S.; Jang, H.; Wang, J.; Qin, Q.; Liu, X.; Cho, J. Bimetallic metal-organic framework-derived MoFe-PC microspheres for electrocatalytic ammonia synthesis under ambient conditions. *J. Mater. Chem. A.* **2020**, *8*, 2099-104. DOI
63. Fernández, S.; Mercado, A.; Cuara, E.; Yeverino-miranda, C.; Sierra, U. Asphalt as raw material of graphene-like resources. *Fuel* **2019**, *241*, 297-303. DOI
64. Romero-sarria, F.; Bobadilla, L.; Jiménez, B. E.; Odriozola, J. Experimental evidence of HCO species as intermediate in the fischer tropsch reaction using operando techniques. *Appl. Catal. B. Environ.* **2020**, *272*, 119032. DOI
65. Ma, M.; Dai, L.; Xu, J.; Liu, Z.; Ni, Y. A simple and effective approach to fabricate lignin nanoparticles with tunable sizes based on lignin fractionation. *Green. Chem.* **2020**, *22*, 2011-7. DOI
66. Yu, B.; Park, K.; Jang, J.; Goodenough, J. B. Cellulose-based porous membrane for suppressing Li dendrite formation in lithium-sulfur battery. *ACS. Energy. Lett.* **2016**, *1*, 633-7. DOI
67. Adams, R. A.; Varma, A.; Pol, V. G. Mechanistic elucidation of thermal runaway in potassium-ion batteries. *J. Power. Sources.* **2018**, *375*, 131-7. DOI
68. Ouyang, Q.; Wang, X.; Wang, X.; Huang, J.; Huang, X.; Chen, Y. Simultaneous DSC/TG analysis on the thermal behavior of PAN polymers prepared by aqueous free-radical polymerization. *Polym. Degrad. Stabil.* **2016**, *130*, 320-7. DOI
69. Zhang, X. Q.; Chen, X.; Cheng, X. B.; et al. Highly stable lithium metal batteries enabled by regulating the solvation of lithium ions in nonaqueous electrolytes. *Angew. Chem. Int. Ed.* **2018**, *57*, 5301-5. DOI
70. Yu, H.; Chen, Y.; Wang, H.; et al. Engineering multi-functionalized molecular skeleton layer for dendrite-free and durable zinc batteries. *Nano. Energy.* **2022**, *99*, 107426. DOI
71. Tie, Z.; Liu, L.; Deng, S.; Zhao, D.; Niu, Z. Proton insertion chemistry of a zinc-organic battery. *Angew. Chem. Int. Ed.* **2020**, *59*, 4920-4. DOI
72. Ye, Z.; Xie, S.; Cao, Z.; et al. High-rate aqueous zinc-organic battery achieved by lowering HOMO/LUMO of organic cathode. *Energy. Storage. Mater.* **2021**, *37*, 378-86. DOI
73. Chen, Z.; Cui, H.; Hou, Y.; et al. Anion chemistry enabled positive valence conversion to achieve a record high-voltage organic cathode for zinc batteries. *Chem* **2022**, *8*, 2204-16. DOI
74. Amanchukwu, C. V.; Kong, X.; Qin, J.; Cui, Y.; Bao, Z. Nonpolar alkanes modify lithium-ion solvation for improved lithium deposition and stripping. *Adv. Energy. Mater.* **2019**, *9*, 1902116. DOI